AN EXPERIMENTAL DYNAMIC METHOD OF INVESTIGATION OF COUNTER-CURRENT ABSORPTION OF OXYGEN IN WATER IN A PACKED BED COLUMN

Pavel MORAVEC and Vladimír STANĚK

Institute of Chemical Process Fundamentals,
Czechoslovak Academy of Sciences, 165 02 Prague 6-Suchdol

Received July 28th, 1986

An experimental method and technique are described in the paper of simultaneous detection of the transfer functions outlet-gas-stream-to-inlet-gas-stream and outlet-liquid-stream-to-inlet-gas-stream for the absorption of oxygen into water in a counter-current packed bed column. Both transfer functions were simultaneously monitored by means of three oxygen electrodes operating on the polarographic principle. The signals of these electrodes were processed in three steps to yield parameters of the model of physical absorption of gas. The first step was on-line evaluation of the Fourier coefficients of the principal harmonic component in all three monitored streams. The second step was the calculation of the frequency characteristics of both transfer functions while the third step yielded parameters of the model by optimization in the frequency domain. The method permits simultaneous evaluation of the parameters of the flow of both phases in the column and the interfacial transfer of oxygen.

Numerous experimental works and practical experience show that in practice so far most extensively used model of the plug flow is not suitable for description of the dynamics of the flow of the gas and the liquid phase in packed bed columns. Various more complex models have been therefore proposed accounting for the effect of the phenomena summarily referred to as longitudinal mixing. Parameters of these models have been determined by static or dynamic experimental methods.

Static methods utilize concentration profile along the column to evaluate the parameters. Although measurement of steady state profiles appears undoubtedly an advantage of the static methods, the difficulties associated with the measurement of these profiles without disturbing the structure of the layer and the flow in the layer are, as a rule, so large as to give an edge to the dynamic methods.

Dynamic methods may be divided into the moment and regression methods. The moment methods are mathematically and computationally relatively simple but insufficiently accurate for more sophisticated models with interfacial mass transfer. The regression methods are more accurate but computationally more exacting. The parameter evaluation may be carried out in the time, Laplace or frequency domain. The advantage of working in the Laplace or frequency domain is that solution of the model equations is substantially simpler than in the time

domain and does not require convolution. An interesting, yet little used, alternative of evaluation was proposed by Kramers and Alberda[1]. Instead of the usual impulse or a step change they used a periodic inlet signal and evaluated the amplitude ratio and the phase angle of the inlet and the outlet signal for several frequencies of the inlet signal. A similar approach was used by Staněk and Čársky[2] who evaluated the model parameters by an optimization routine based on an objective function combining the real and the imaginary part of the frequency characteristic into the form

$$\psi = \sum_{j=1}^{N} \{[R_t(\omega_j) - R_e(\omega_j)]^2 + [I_t(\omega_j) - I_e(\omega_j)]^2\} . \qquad (I)$$

Dynamic methods have been used so far almost exclusively in combination with a tracer which does not cross the interface. Hence they could be used only for the study of the dynamics of the flow of that phase in which the concentration signal had been generated. With the aid of tracers that cross the interface one can study, in principle, simultaneously the dynamics of the flow of both phases including that of the interfacial mass transfer. In the previous paper[3] we have formulated a model of a counter-current absorption of a poorly soluble gas, consisting of the axially dispersed model for the gas phase (AD) and the axially dispersed model with stagnant zone (PDE – piston diffusion exchange) for the liquid phase[4]. Theoretical expressions for the transfer functions have been derived for this model and its three limiting cases.

The aim of this paper has been to test the applicability of the dynamic method of measurement and data evaluation in the frequency domain for simultaneous evaluation of the parameters of the model of the flow of the gas and the liquid phase with interfacial mass transfer during counter-current absorption of oxygen into water in a packed bed column.

EXPERIMENTAL

Experimental Set-up

The results of the previous study[3] have shown that during absorption of a poorly soluble gas in a relatively tall trickle bed column one can utilize, for the evaluation of the model parameters, only the transfer functions X_{GZ}/X_{G0} (outlet-gas-stream-to--inlet-gas-stream) and X_{L0}/X_{G0} (outlet-liquid-stream-to-inlet-gas-stream), or their frequency characteristics.

For the experiments of this type an experimental set-up was constructed, shown schematically in Fig. 1. The column *1* was a perspex glass tube 0·105 m in internal diameter, packed to a height of 2·1 m by glass spheres 0·01 m in diameter. The voidage of this layer was 0·4. The layer was irrigated by water trickling down counter-

-currently to the flowing air with periodically variable concentration of oxygen serving as an absorbed species. On the basis of the previous theoretical analysis[3], oxygen may be regarded as a gas poorly soluble in water.

The periodic signal of oxygen concentration in the form of approximately rectangular pulses was generated in the inlet gas stream by means of three parallel branches AIR1, AIR2, O2 merging just before the column gas inlet end *4*. The main stream of air AIR1, which was permanently fed into the column, was supplemented by either the auxiliary air stream AIR2 or the stream O2 carrying the tracer; the tracer being either oxygen or nitrogen. These two auxiliary branches were equipped with solenoid valves S1, S2 and their alternative opening and closing caused that the main stream of air was mixed in the first half-period with air while in the second half-period with either oxygen or nitrogen. This provided a periodic inlet signal while the overall flow rate of gas through the column remained constant. The operation of the solenoids was controlled by a dual time relay CR with an adjustable length of the half-period of the inlet signal.

The time course of oxygen concentration was monitored by means of oxygen electrodes of the polarographic type (manufactured by Development Workshops, Czechoslovak Academy of Sciences) in the inlet gas stream (E1 in Fig. 1), in the outlet gas stream E2, and in the outlet liquid stream E3. Current feed for the three electrodes and conversion of their signal to a voltage signal was provided by a pair of two-channel Oxymetr instruments, of the same manufacturer, shown in Fig. 1 as OX1 and OX2. The analog signals were processed by a computing data logger ADIMES and the results were recorded on a paper tape PTP and a typewriter TW.

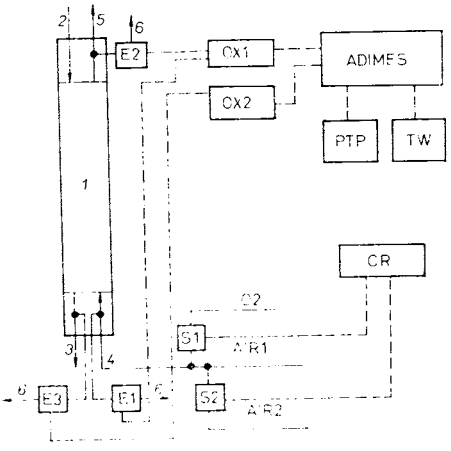

FIG. 1

Scheme of experimental set-up. *1* column, *2* inlet water stream, *3* outlet water stream, *4* inlet gas stream, *5* outlet gas stream, *6* outlet stream of sampled gas or water. E1, E2, E3 oxygen electrodes, OX1, OX2 two-channel Oxymetr instruments, S1, S2 solenoid valves, CR solenoid valves controling relays, AIR1 steady main stream of air, AIR2 auxiliary stream of air, O2 oxygen or nitrogen stream, ADIMES computing data logger, PTP paper tape punch, TW typewriter

Sampling of the Streams of Both Phases

During dynamic measurements it is important to protect the signal from undue distortion by the dynamics of the probe itself by the end effect of the column, or by the method of sampling the stream. For this reason the sampling port for the inlet gas stream was located as close as possible to the bottom of the packed layer (1 cm), in order to minimize the volume between the two locations. Also the volumes of tubings leading the sampled stream to the cells with the measuring electrodes were minimized. The arrangement of the sampling system for the outlet and the inlet gas was identical; identical flow rates of sampled streams were ensured by a pair of identical magnetic gas pumps.

The need to prevent entrainment of liquid into the sampled gas during intensive regimes of column operation led us to locating the sampling port for the outlet gas about 15 cm above the packed layer. The measure caused later difficulties in the modelling of the effect of this space on the dynamics of the process.

The most complicated task proved to be the sampling of the outlet liquid stream. For liquid, as a discontinuous phase, it was rather difficult to meet two contradicting requirements, *i.e.* to sample sufficiently strong stream of liquid averaged over the column cross section, yet not averaged in time. The scheme of the sampling device used is shown in Fig. 2. A substantial fraction of the liquid outlet stream trickles down a sampling fin *4* into a funnel *5* and from here, by gravity, to a measuring cell *6* housing the oxygen electrode. The funnel *5* was constructed so as to have a minimum holding volume *per* unit area of collecting surface.The flow rate of the sampled liquid was regulated to a maximum possible level, which, however, did not bring about entrainment of gas bubbles into the measuring cell with the electrode. The sampling fin represents at the same time the principal rib of the supporting grid.

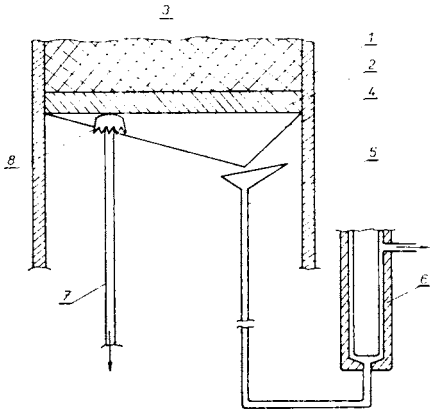

FIG. 2

Sketch of the device for continuous sampling of the liquid phase below the column grid. *1* column, *2* grid, *3* packing, *4* sampling fin, *5* funnel, *6* cell with electrode, *7* tubing for sampled gas phase, *8* cap preventing penetration of liquid into sampled gas stream

The sampling fin, however, differs from the remaining ribs of the grid by its enlarged vertical size.

Oxygen Electrodes

Oxygen electrode is a device the signal of which is proportional to the fugacity of oxygen on the surface of the catode. The electrode thus appears suitable for measurement of oxygen concentration both in the gas and the liquid phases as the signal of the electrode in the liquid saturated by oxygen is the same as in the gaseous oxygen. It is immaterial that the concentration of oxygen in the liquid phase is substantially less than in the gas phase (in equilibrium m-times).

The oxygen electrode, however, is not a probe with an instantaneous response and if it is to be used for measurement of the dynamics of relatively rapid processes, it is necessary to determine its dynamic characteristics[5]. For description of the dynamics of the electrode we used the so-called two-zone model described in ref.[6]. To this choice led us the earlier published[7] experience. The parameters of the two--zone model were evaluated from independent measurements of the frequency characteristics of the oxygen electrode. An example of the experimental frequency dependence of the amplitude of the signal of the electrode alone and its approximation by the above-mentioned model is shown in Fig. 3. Apart from the measurement of the dynamics of the oxygen electrode it was necessary to carry out also their static calibration. In contrast to the measurement of the dynamics, the static calibration constituted part of the measurement of the dynamics of the absorption. The oxygen electrodes were in this case placed in their measuring cells connected to the absorption column. The static calibration consisted in the measurement of the

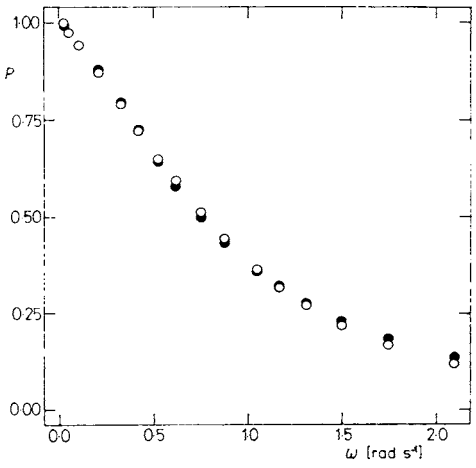

FIG. 3

Frequency dependence of the amplitude ratio of the signal of oxygen electrode. ○ experimental values; ● computed dependence from the model

signals of the electrodes under the steady state conditions of absorption and the following limiting oxygen concentrations: The concentration of oxygen in air, in water saturated by air, in the air–tracer mixture, and in water saturated by this mixture. All calibrations were carried out at the temperature and pressure of the dynamic experiment. This method of calibration was based on the following two assumptions:

a) The concentration of oxygen in the gas stream does not change on passing through the column.

b) On passing through the column the liquid is saturated to equilibrium value.

For our absorption system, column length, and investigated ranges of flow rates of both phases, both these assumptions are believed to be well satisfied.

Static calibration was carried out for each frequency characteristic three times: At the beginning, approximately in the middle, and at the end of the experimental series.

The Measurement of the Dynamics of Oxygen Absorption

The experiment proper consisted of the measurement of time courses of the signals of the three above-mentioned electrodes (the concentrations of oxygen in both gas streams and the exit liquid stream) for preselected number of frequencies of the inlet oxygen concentration signal. In our experiments the number of frequencies for a single regime of absorption (given by the flow rates of both phases) ranged between 10 and 18, depending on the rate of damping the amplitude of the outlet signals. The measurements were always carried out starting from the lowest frequency toward the highest one.

The flow rates of oxygen or nitrogen in the branch O2 in Fig. 1, which created the concentration signal, were selected so as to have the difference between the readings of signals of the oxygen electrodes under the steady state limiting concentrations at least 0·2 volts with the maximum range of readings being between 0 and 1 V.

The temperature of the liquid phase was $20 \pm 0{\cdot}5°C$. The gas phase was not thermostated; its temperature at the column inlet was close to the laboratory temperature, the latter being usually 2–3°C higher than the temperature of the liquid phase. The flow rates of the sampled gas phase at the column inlet and outlet were in all experiments identical and equal to $1{\cdot}67 \cdot 10^{-5}$ m^3 s^{-1}. The flow rates of the sampled liquid phase ranged between $1{\cdot}31 \cdot 10^{-6}$ and $6{\cdot}8 \cdot 10^{-6}$ m^3 s^{-1}, depending on the flow rate of the liquid phase in the column.

THEORETICAL

The evaluation of data was carried out in three steps using the harmonic analysis, the Fourier transform, and optimization in the frequency domain.

On-line Fourier Transform

A periodic signal $c(t)$, with an angular velocity omega, may be expressed by a Fourier series as

$$c(t) = a_0 + \sum_{k=1}^{\infty} [a_k \cos(k\omega t) + b_k \sin(k\omega t)] . \qquad (2)$$

In the processing of a periodic signal, satisfying the Dirichlet conditions[8], one can consider this signal as being composed of individual harmonic components. If the process under investigation is linear, an arbitrary component may be selected for the analysis of the signal transfer. The best, naturally, appears the one whose amplitude is maximal. For the case of our signal it is the frequency for $k = 1$ in Eq. (2).

For the numerical evaluation of the coefficients a_0, a_1, and b_1 it is useful to split the period of the signal, T, to n equal intervals with initial time coordinates

$$t(j) = jT/n , \quad j = 0, 1, \ldots, n - 1 \qquad (3)$$

indicating the instants of measurement of the signal $c(t)$. Under the simultaneous detection of three signals it is necessary that n be a multiple of 3. Having made the substitution $\omega = 2\pi/T$ one can write for the sought coefficients the following expressions in discrete form:

$$a_{0i} = \frac{3}{n} \sum_{j=0}^{n/3-1} c_i(3j + i - 1) \qquad (4)$$

$$a_{1i} = \frac{6}{n} \sum_{j=0}^{n/3-1} c_i(3j + i - 1) \cos [2\pi(3j + i - 1)/n] \qquad (5)$$

$$b_{1i} = \frac{6}{n} \sum_{j=0}^{n/3-1} c_i(3j + i - 1) \sin [2\pi(3j + i - 1)/n] , \qquad (6)$$

where the subscript $i = 1, 2, 3$ differentiates between the signals of individual oxygen electrodes **E1**, **E2**, **E3**.

The coefficients a_{0i}, a_{1i}, and b_{1i} were computed on-line in the course of measurements by the computing data logger **ADIMES** (Fig. 1) and on completion of the experiment were, together with the remaining data, punched onto a paper tape. The direct result of on-line preprocessing of data by **ADIMES** were thus, for the given regime of absorption, determined by the flow rates of phases, the Fourier coefficients of the concentration signals of the three measured streams for the set of given frequencies of the inlet signal.

Evaluation of the Experimental Transfer Characteristics of the Absorption Column

In the second step the previously obtained Fourier coefficients served to calculate the amplitudes from

$$A = (a_1^2 + b_1^2)^{0.5} \tag{7}$$

and the phase angles from

$$\Phi = \text{arctg}\,(b_1/a_1) \tag{8}$$

for individual signals. The amplitudes, computed from Eq. (7), were then normalized by amplitudes corresponding to the zero frequency (obtained by measurement of limiting concentrations of oxygen under the steady state) to obtain the amplitude ratios P_1, P_2, P_3 for the signals measured by the electrodes **E1**, **E2**, **E3**.

The method of calculation of the transfer functions X_{GZ}/X_{G0} and X_{L0}/X_{G0} from the amplitude ratios and phase angles of the signals of the electrodes **E1**, **E2**, and **E3** is apparent from Fig. 4. The experimental signals reflect not only the response of the process in the absorption column itself but also the deformation of the signals during transportation of the sampled streams to the electrodes and the distortion of the signals by the oxygen electrodes themselves. The spaces between the location of the sampling port for the gas phase and the bottom or the upper end of the packed layer, **VK1** and **VK2**, were modelled by the plug flow, equally as the volumes of the tubings to the measuring cells, **VE1**, **VE2**, and **VE3**. The frequency characteristics of the oxygen electrodes were evaluated from independent measurements.

Using Fig. 4 one can formulate the following transfer relations for the electrodes **E1**, **E2**, and **E3**.

$$F_1 = F_{VE1} \cdot F_{E1} \tag{9}$$

$$F_2 = F_{VK1} \cdot X_{GZ}/X_{G0} \cdot F_{VK2} \cdot F_{VE2} \cdot F_{E2} \tag{10}$$

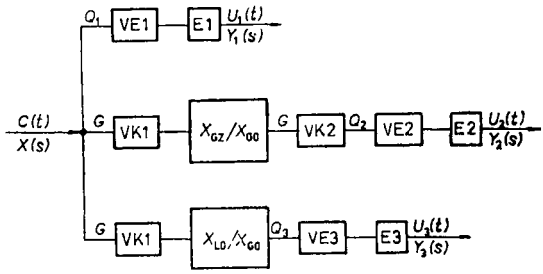

FIG. 4
Scheme of corrections of the measured signals

$$F_3 = F_{VK1} \cdot X_{L0}/X_{G0} \cdot F_{VE3} \cdot F_{E3}. \qquad (11)$$

Since the transfers F_1 to F_3 represent overall transfers of elements in series, the amplitude ratios of the overall transfers P_1 to P_3 are given as products of the amplitudes of partial elements while the phase lags Φ_1 to Φ_3 are equal to the sums of partial phase lags.

From the amplitude ratios P_2/P_1 and P_3/P_1 and the phase lags $\Phi_2 - \Phi_1$ and $\Phi_3 - \Phi_1$ one can determine the amplitude ratios and phase lags of the transfer functions X_{GZ}/X_{G0} and X_{L0}/X_{G0}

$$P(X_{GZ}/X_{G0}) = (P_2 \cdot P_{E1})/(P_1 \cdot P_{E2}) \qquad (12)$$

$$P(X_{L0}/X_{G0}) = (P_3 \cdot P_{E1})/(P_1 \cdot P_{E3}) \qquad (13)$$

$$\Phi(X_{GZ}/X_{G0}) = \Phi_2 - \Phi_1 - (\Phi_{VK1} + \Phi_{VK2}) \qquad (14)$$

$$\Phi(X_{L0}/X_{G0}) = \Phi_3 - \Phi_1 + (\Phi_{VE1} - \Phi_{VE3}) - \Phi_{VK1}. \qquad (15)$$

In Eqs (*12*)–(*15*) we have taken into account the fact that the amplitude ratios corresponding to the plug flow equal unity, and further the that phase lags Φ_{VE1} and Φ_{VE2} were identical under our experimental conditions. Figs 5 and 6 show for illustration the amplitude ratios and phase lags of the transfer functions X_{GZ}/X_{G0} and X_{L0}/X_{G0} in dependence on the frequency of the input concentration signal for experiments K032 and K046.

The experimental conditions for these two experiments were as follows: K032: $L = 0{\cdot}00409$ m s^{-1}; $G = 0{\cdot}268$ m s^{-1}, K046: $L = 0{\cdot}0151$ m s^{-1}; $G = 0{\cdot}0545$ m s^{-1}. The different experimental conditions reflect in the course of the Bode diagrams of both of these experiments while the results are more conspicious for the transfer function X_{GZ}/X_{G0}, see Fig. 5. The amplitude ratio of the transfer function X_{GZ}/X_{G0} for the experiment K032, *i.e.* for the high gas flow rate, is damped little, which signalizes the character of the gas flow as being close to the plug flow. At low gas rate and high liquid flow rates (experiment K046) the amplitude ratio, on the contrary, is damped strongly, a fact that hints at intensive longitudinal mixing of gas. The dependence of the phase lag of the transfer function X_{GZ}/X_{G0} on angular velocity displays for experiment K032 nearly linear course, which again corresponds to the character of the plug flow of the gas phase. The differences between experiments K032 and K046 are mainly due to the different gas flow rates and different gas hold-ups for the two experiments.

For the transfer function X_{L0}/X_{G0}, see Fig. 6, the character of the Bode diagrams is substantially different compared to that of the diagrams for the transfer function X_{GZ}/X_{G0}. The difference between the experiments K032 and K046 is now substantially smaller. The amplitude ratio is damped substantially more than in case of the

transfer function X_{GZ}/X_{G0} and the dependence of the phase lag on the angular velocity displays strongly nonlinear character. The magnitude of the amplitude ratio is higher for the experiment K046 and the magnitude of the phase lag in absolute value, on the contrary, for the experiment K032.

The real and the imaginary parts of the transfer functions may be computed from the known values of the amplitude ratios and phase lags, *i.e.* from

$$R = P \cos \Phi \tag{16}$$

$$I = P \sin \Phi \,. \tag{17}$$

The values of the transfer functions X_{GZ}/X_{G0} and X_{L0}/X_{G0}, computed in this way for individual values of the frequency of the signal, *i.e.* the frequency characteristics, are plotted in Figs 7 and 8. The Bode diagrams provide a better illustration of the changes of the signal upon passing through the equipment; for parameter evaluation appear more suitable the characteristics in the complex plane where the contribution

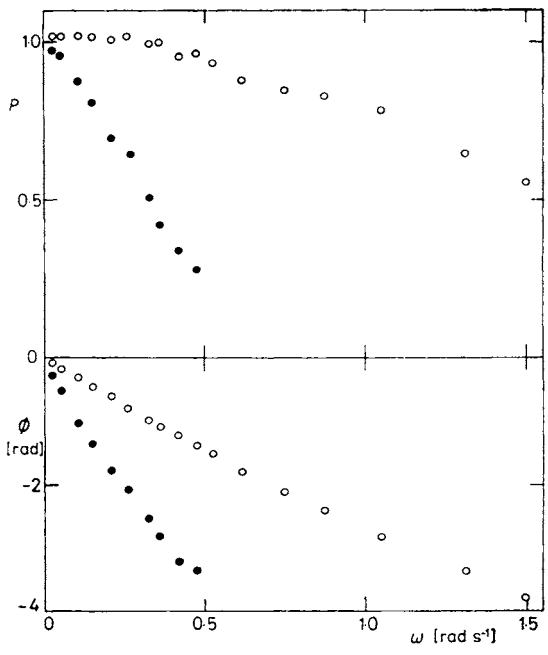

FIG. 5

Bode diagrams of the transfer function X_{GZ}/X_{G0}. ○ K032; ● K046

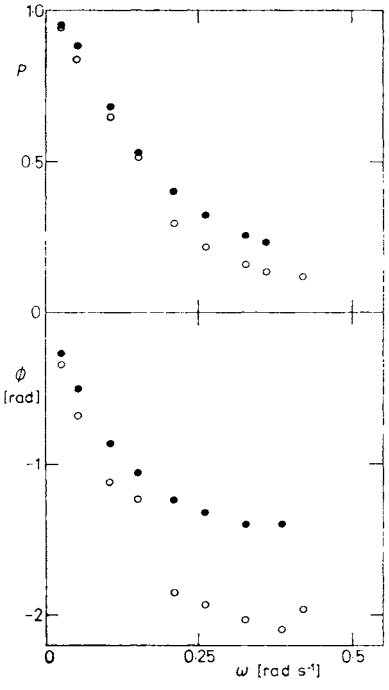

FIG. 6

Bode diagrams of the transfer function X_{L0}/X_{G0}. ○ K032; ● K046

of the amplitude ratio and the phase lag is in a way normalized to a comparable magnitude. The frequency characteristics of the transfer fuhctions X_{GZ}/X_{G0} and X_{L0}/X_{G0} were the result of the second step of data processing.

Optimization of the Model Parameters from the Frequency Characteristics

The evaluation of the parameters of the employed models from the experimental frequency characteristics of the transfer functions X_{GZ}/X_{G0} and X_{L0}/X_{G0} was carried out on an EC 1033 computer using the Marquardt optimization technique[9]. The optimization was carried out with the aim to utilize information in both transfer functions by formulating an objective function in the form:

$$\psi = \sum_{j=1}^{M} \{[R_t(\omega_j) - R_e(\omega_j)]^2 + [I_t(\omega_j) - I_e(\omega_j)]^2\}_{X_{GZ}/X_{G0}} + \\ + \sum_{j=1}^{N} \{[mR_t(\omega_j) - R_e(\omega_j)]^2 + [mI_t(\omega_j) - I_e(\omega_j)]^2\}_{X_{L0}/X_{G0}} . \qquad (18)$$

In order to give both transfer functions approximately the same weight, the theoretical values of the transfer function X_{L0}/X_{G0} (*i.e.* the real and the imaginary part R_t, I_t) were multiplied by the constant m. The experimental data need not have been modified in this way for the signal of the oxygen electrode in the liquid phase cor-

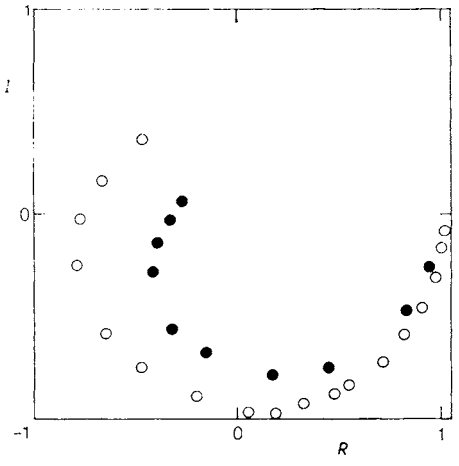

FIG. 7

Frequency characteristics of the transfer function X_{GZ}/X_{G0}. ○ K032; ● K046

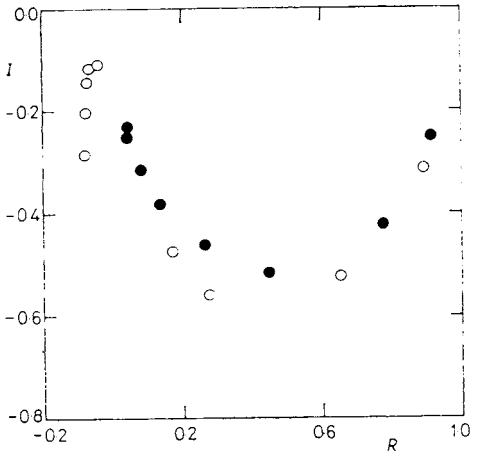

FIG. 8

Frequency characteristics of the transfer function X_{L0}/X_{G0}, ○ K032; ● K046

responded to the fugacity of the dissolved oxygen and, hence, it was exactly m-times higher than the oxygen concentration in the liquid phase.

The number of measurements M and N of the transfer functions X_{GZ}/X_{G0} and X_{L0}/X_{G0}, respectively, was generally different as the evaluation was always carried out only for those frequencies for which the amplitude of the outlet signal reached at least 10% of the amplitude at zero frequency and the rates of damping for the two cases were different.

The evaluation of the parameters was carried out for the original eight-parameter model[3] and its limiting cases: The axially dispersed model in both phases (AD–AD), the model consisting of the cross flow model in the liquid phase (PE – piston exchange[10]) and the axially dispersed model (AD) in the gas phase (PE–AD), and the plug flow model in both phases.

Figs 9 and 10 show theoretical dependences of the transfer functions X_{GZ}/X_{G0} and X_{L0}/X_{G0} of the principal model on frequency together with the experimental data for the expeiment K046. The agreement of the model curves with the experimental data is quite good. Particularly for the transfer function X_{L0}/X_{G0}. The applicability of individual models tested and the obtained values of parameters shall be subject of the next communication.

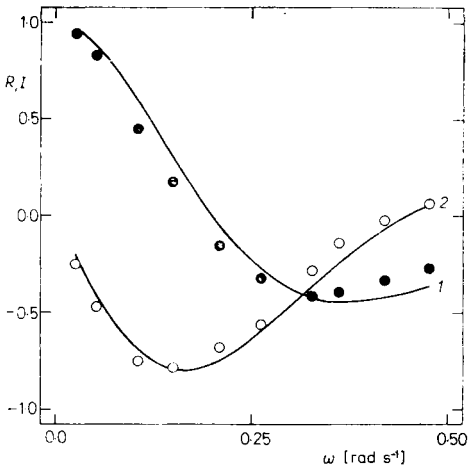

FIG. 9

Comparison of the theoretical frequency characteristic of the transfer function X_{GZ}/X_{G0} for the PDE–AD model with experimental data, experiment K046. *1 R*; *2 I*

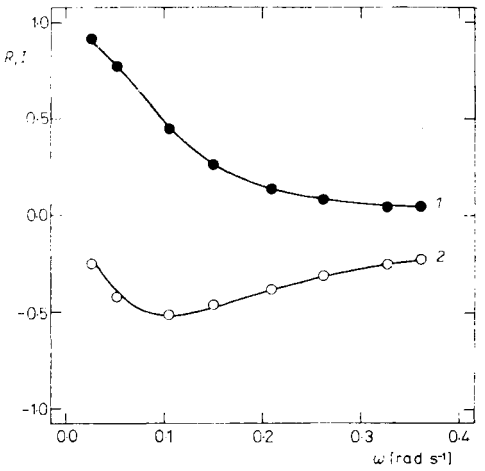

FIG. 10

Comparison of the theoretical frequency characteristic of the transfer function X_{L0}/X_{G0} for the PDE–AD model with experimental data, experiment K046. *1 R*; *2 I*

DISCUSSION

The undoubted advantage of the presented experimental method is the simultaneous measurement of the response in both outlet streams and thereby the possibility of simultaneous study of the flow of both phases including interfacial mass transfer. Practical realization of the experiment is relatively simple, the experimental instruments are easily available and both the amount of the experimental work and computational effort involved are at an acceptable level. Application to other systems, however, fundamentally depends on the availability of the probe measuring the concentration of the absorbed component in both phases with necessary dynamic properties and accuracy.

From Figs 5 and 6 it is apparent that the response of the equipment for both transfer functions is sufficiently marked as far as the amplitude ratio is concerned. The phase lag for the transfer function X_{L0}/X_{G0} is substantially smaller, which increases the requirements on the accuracy of measurements. This is documented by the higher scatter of the phase lag of the transfer function X_{L0}/X_{G0} in Fig. 6. As important also appears the fact that the frequency ranges of the measurable frequency response for the two transfer functions are considerably different (depending on the experimental conditions). Special attention must be paid to this fact in the planning the experiment.

A certain problem in applying dynamic methods is posed by the distortion of the signal by the end effects and due to the imperfect dynamics of the measuring probe. Figs 9 and 10 seem to suggest that in spite of the implemented corrections these effects had not been perfectly eliminated. Special attention has to be devoted to minimizing the end volumes rather than to the improvement of their modeling.

Solution of the balance equations in the Laplace domain cosiderably simplified matters and, in fact, enabled analytical solution of the whole set, with the exception of the solution of the characteristic equation. Even then, though, the computer time used for optimization was, except the case of the plug flow in both phases, not negligible. The average time of optimization for a single experiment amounted to 15 seconds for the plug flow model, but for the remaining models amounted to 1 000–2 500 seconds. The optimization in the time domain would then, no doubt, require a faster computer.

Finally one can conclude that the presented method of measurement and data processing may be well employed to obtain the frequency characteristics of the transfer functions X_{GZ}/X_{G0} and X_{L0}/X_{G0} for simultaneous evaluation of the dynamics of the flow of both phases including interfacial mass transfer.

LIST OF SYMBOLS

A	amplitude
a_k	coefficient of the Fourier transform
a_0	coefficient of the Fourier transform
b_k	coefficient of the Fourier transform
c	concentration, kmol m^{-3}
F	transfer function
G	gas velocity, m s^{-1}
I	imaginary part of the transfer function
L	liquid velocity, m s^{-1}
m	equilibrium constant of oxygen solubility
N	number of measurements
n	total number of samplings of the signal in the course of a single period by all three electrodes
P	amplitude ratio
Q	velocity of gas or liquid through the measuring cell, m s^{-1}
R	real part of the transfer function
T	period, s
t	time, s
U	signal of the oxygen electrode
X	Laplace transform of oxygen concentration
Y	Laplace transform of signal U
Φ	phase lag, rad
ψ	objective function
ω	angular velocity, rad s^{-1}

Subscripts

E1	electrode in inlet gas stream
E2	electrode in exit gas stream
E3	electrode in exit liquid stream
e	experimental value
G	gas phase
L	liquid phase
t	theoretical value
VE1	tubing leading to electrode E1
VE2	tubing leading to electrode E2
VE3	tubing leading to electrode E3
VK1	end space below the bottom end of packing
VK2	end space above the top of packing
Z	top of the packed section
0	bottom of the packed section
1	inlet gas stream
2	outlet gas stream
3	outlet liquid stream

REFERENCES

1. Kramers H., Alberda G.: Chem. Eng. Sci. *2*, 173 (1953).
2. Staněk V., Čársky M.: Collect. Czech. Chem. Commun. *48*, 258 (1983).
3. Moravec P., Staněk V.: Collect. Czech. Chem. Commun. *51*, 1222 (1986).
4. van Swaaij W. P. M., Charpentier J. C., Villermaux J.: Chem. Eng. Sci. *24*, 1083 (1969).
5. Moravec P.: *Thesis.* Institute of Chemical Process Fundamentals, Czechoslovak Academy of Sciences, Prague 1983.
6. Linek V., Beneš P., Vacek V.: Ind. Eng. Chem., Fundam. *18*, 240 (1979).
7. Linek V., Moravec P.: Sb. Vys. Sk. Chem.-Technol. Praze K*13*, 61 (1978).
8. Angot A.: *Applied Mathematics for Electronical Engineers* (in Czech). Published by SNTL — Nakladatelství technické literatury, Prague 1972.
9. Marquardt D. M.: J. Soc. Ind. Appl. Math. *11*, 431 (1963).
10. Hoogedoorn C. J., Lips J.: Can. J. Chem. Eng. *43*, 125 (1965).

Translated by the author (V.S.).